*Optica Applicata, Vol. XXXI, No. 2, 2001*

# Manufacturing and characterization of ring-index optical fibers

RYSZARD S. ROMANIUK

Institute of Electronic Systems, Warsaw University of Technology, Nowowiejska 15/19, 00–665 Warszawa, Poland.

This work analyses theoretically, technologically and practically a class of low-loss single-mode optical fibers with ring refractive index profile. The fibers are considered for long distance signal transmission as well as photonic signal processing. Trunk transmission, ring-index fibers have shifted and flattened dispersion characteristics and much larger effective area as compared with standard step-index single-mode. Signal processing, device oriented, ring-index fibers have a unique capability of transmitting either quasi planar modes for large ring diameters or the second order mode in a quasi single-mode regime at lossy discrimination of the fundamental mode, for small ring diameters. Theoretically predicted features of single-mode ring-index fibers were confirmed experimentally on samples prepared by the author.

## 1. Introduction

Standard step-index single-mode optical fibers, which are telecommunications oriented, have attenuation in the range of 0.3 dB/km for 1310 nm and below 0.2 dB/km for 1550 nm. The dispersion is around zero and 17 ps/nm×km (with the slope 80 fs/nm$^2$×km) for respective transmission windows (Fig. 1). The latter level is unacceptable for high-speed transmission. Control of refractive index profile effectively changes the waveguide component of fiber dispersion and mode-field diameter (Fig. 2) [1]. Depending on the way the dispersion and effective area are influenced by the index profile, one uses the following names for these high performance, optical fibers:

– zero dispersion shifted, for the same characteristics as standard single-mode, but with zero dispersion in the second window,

– nonzero dispersion shifted, for the same characteristics as standard single-mode, but with zero dispersion either around 1450 nm or above 1600 nm,

– reduced slope, for characteristics crossing zero dispersion at a considerably reduced slope in comparison with standard step-index single-mode, typically below 50 fs/nm$^2$×km,

– flattened, for characteristics crossing zero for two or even three wavelengths in the usable transparency region,

– large effective area, dispersion shifted.

Dense wavelength division multiplexing (DWDM) systems, now with 10 or 40 Gbit signals packed every 25 or 50 GHz, imposed additional requirements of their own on novel fiber generations [2]. The key fiber parameters to be adjusted are not only the dispersion characteristics (magnitude and slope inside a window) but also effective area (or mode field diameter) of the fiber. Controlled low level of dispersion combined with large effective area combats nonlinear effects in trunk systems [3]. The DWDM channels are spaced uniformly, so the frequency from, accumulated over long distance, four-wave mixing can interfere with adjacent channel causing noise and system degradation. Very low dispersion causes the signals to stay in phase over long distances. On the contrary, controlled dispersion spreads out the signals, reducing considerably their phase interaction. Now, the balance seems to be in the region of a few single ps/nm×km [3], [4]. On the other hand, the dispersion slope has to be reduced, in the whole transmission window now spanning over 100 nm in a variety of practical systems [2], to equalize the differential characteristics. The future requirements, in this respect, seem to be even more demanding with the $L$ band systems finishing their laboratory and developmental stages [2]. It is foreseen [2] that the "all-wave", low-hydrogen, fiber systems will work in the uninterrupted window spanning from 1250 nm up to 1700 nm. These requirements lead to fibers with reduced dispersion slope and increased nonlinearity levels to extend their operating bandwidth.

This work shows theoretically and practically that some of the above-mentioned requirements are fulfilled by specially designed representatives of ring-index class optical fibers, though the presented results of calculations and measurements are of more fundamental nature than required by immediate application processes.

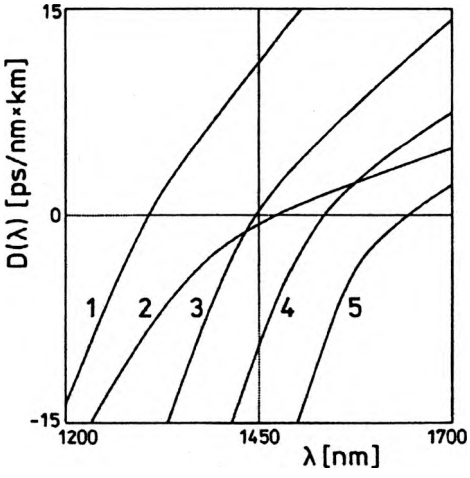


Fig. 1. Calculated dispersion curves $D(\lambda)$ [ps/nm×km] for several types of commercial, optical communications oriented, single-mode fiber. 1 – standard single-mode, 2 – reduced slope, 3 – (positive) nonzero dispersion shifted, 4 – zero dispersion shifted, 5 – (negative) nonzero dispersion shifted. Dispersion flattened fiber is not yet used in commercial optical trunk communications systems. It is tried in the so-called all-wave, metro systems.

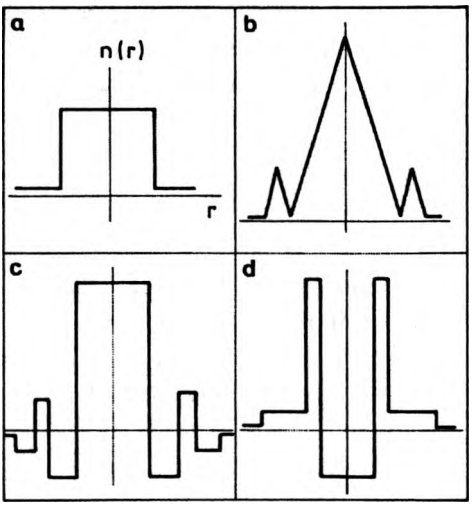


Fig. 2. Schematic representation, depicted not to scale, of refractive index profiles for fibers of different dispersion and modal effective area characteristics. **a** – step-index single-mode (curve 1 in Fig. 1), **b** – dispersion shifted (curves 3–5 in Fig. 1), **c** – reduced slope, quadruple clad (curve 2 in Fig. 1), **d** – dispersion shifted, large effective area, ring-index (for example, curve 3 in Fig. 1, but with larger effective area than for other index profiles).

The major motivation behind this work is that the references of ring-index fibers are fewer and much more modest than for other fibers optimized for photonic signal transmission and processing. This is, perhaps, the reason why the fibers are not yet available off the shelf, but there is every indication [2] of their being intensely prepared for commercialization by several photonic firms. The work starts with some problems connected with the manufacturing of single-mode optical fibers of quite complex refractive index profiles. The signal properties of ring-index fibers were analysed and some of these properties were compared with the results of measurements performed on single-mode and multi-mode fiber samples manufactured during the modifed multicrucible process (MMC process).

## 2. Manufacturing considerations for ring-index optical fibers

A modified multicrucible process (referred to as MMC) was considered here for the manufacturing of ring-index optical fibers [5]–[7]. Fabrication of complex profile fiber requires a strict control of diffusion conditions during the process. The boundary conditions during the preform or fiber pulling are imposed by the ion system and the technology used – geometry, time and temperature. The MMC process gives three kinds of basic classes of index profiles [6]–[8]: multi-step, ring and mixed (*W* or multi-clad). The process starts with a choice of proper ion system susceptible to diffusion and insuring acceptable level of mutual ion mobility. The best modifier for the core is the one which increases the index and is very mobile. A gradient of ion

concentration and, generally, chemical potential is necessary for a directed diffusion stream to occur. The process is intense only in the confined inter-nozzle region, where the core-cladding system of glasses has low viscosity, and can be described by the second Fick's law for cylindrical coordinates

$$\frac{\partial^2 c}{\partial r^2} + \frac{\partial c}{r\partial r} - \frac{1}{D}\frac{\partial c}{\partial t} = 0 \tag{1}$$

where: $c = c(r, t)$ – distribution of modifying ions, $D$ – diffusion constant, $t$ – diffusion time, $r$ – radius. For the boundary conditions $t = 0$, $c(r, t) = C_0$ if $0 < r < a$ and $c(r, t) = 0$ for $r > a$, where $a$ – fiber core radius, $C_0$ – initial ion concentration in source glass, the diffusion equation has the following solution for the concentration distribution of diffusing ion:

$$c(r, t) = C_0 \int_0^{\infty} \exp\left(\frac{Dt}{R^2}u^2\right) J_0\left(-\frac{r}{R}u\right) J_1(u)\,\mathrm{d}u \tag{2}$$

where: $J$ – Bessel function, $2R_r$ – diameter of core nozzle, $2R_p$ – diameter of cladding nozzle, $L_d$ – diffusion length. A normalized diffusion coefficient is defined as $K = Dt/R^2$. It is possible to bind the standard coefficient of ion exchange $K$ with the parameters of technological process. The following equation holds for the flowing glass $R^2 V_{\text{glass}} = a^2 v_{\text{fiber}}$, where $R$ – radius of nozzle, $V_{\text{glass}}$ – velocity of glass flow through core nozzle, $a$ – radius of fiber, $v_{\text{fiber}}$ – velocity of fiber pulling. The value of parameter $K$ is combined with volume glass flow through $K = D\pi L_d/Q_r$, where $Q_r$ – volume flow of core glass. The diffusion length and time are $t_d = L_d/V_{\text{glass}} = L_d R^2/a^2 v_{\text{fiber}}$, thus the normalized diffusion coefficient is $K = DL_d/a^2 v_{\text{fiber}}$. This simplification assumes the profile to be a superposition of $\alpha$-type profiles.

Diffusion of $Pb^{2+}$, $Ba^{2+}$, $K^+$, $Na^+$ ions has been traced in MMC preforms and fibers. The aim was to find the dependencies between the technological process parameters, ion system in core-cladding glasses used, and the resulting index profile in the fiber. The process parameters that influence the diffusion include: zonal temperatures in the divided furnace, construction of crucible pile, lengths of thermal zones, total diffusion length, material constants, *etc*. The ion concentration curves were measured by means of electron microscope probe [6]–[8]. The parameters $D$ and $K$ were calculated from measured concentration profiles using modified Boltzmann–Matano method, adapted for cylindrical geometry [8]. As an example, we calculated here the data for F2-S6 system of core-cladding glasses with $Pb^{2+}$ and $Na^+$ migrating ions. The output data are: mean concentration of $Pb^{2+}$ in the core $C_{\text{core}}^{\text{Pb}} = 17.3\%$, no lead ions in the cladding at the beginning of the process $C_{\text{clad}}^{\text{Pb}} = 0$, diameter of core region $d_{\text{core}} = 2r_{\text{core}} = 100\ \mu\text{m}$, diffusion length $l_d = 32$ mm, pulling speed $v = 50$ m/min, diameter of core crucible nozzle $d_{\text{core}}^{\text{n}} = 2r_{\text{core}}^{\text{n}} = 4$ mm, diffusion

time $t_d = l_d d^n_{core}/v d_{core} = 62$ s, location of Matano plane $X_M = x(1 - C_x/C_c)$, where: $x$ is the radial coordinate here, $C_c$ – output ion concentration in the core, $C_x$ – local ion concentration along radius of fiber cross-selection. From the measured ion concentration profile $C = f(x/r_{core})$ one obtains, for a particular MMC preform analyzed, $x/r_{core} = 0.7$, $C_x/C_r = 0.8$, $x = 35$ μm, and further $X_M = 7$ μm, $C_x = 14\%$mol. The Boltzman–Matano equation allows the values of $K$ and $D$ to be calculated:

$$D_{Pb} = -\frac{1}{2t_d}\left(\frac{dx}{dC}\right)\Bigg|_x \int_{C_r}^{C_x}(X - X_M)dC = 1.5\times10^{-5}\frac{cm^2}{s},$$

$$K_{Pb} = \frac{Dl_d}{r^2_{core}v} = 2.2 \times 10^{-2}. \tag{3}$$

The respective values for Na ions are: $D_{Na} = 5 \times 10^{-5}$ cm$^2$/s, $K_{Na} = 8 \times 10^{-2}$. The differences of diffusion parameters between both ions are not very big, despite the considerable difference in sizes. This is caused by the mixed alkali effect introduced by the presence of $K^+$ ions in the core glass. The mobility of $Na^+$ ions is considerably reduced by this effect. The result is that the heavy ions determine the index profile, which can be shaped very precisely. The resulting index profiles in fiber samples were measured by interference method. Analogous investigations of diffusion were conducted for other ion systems and typical glasses for the MMC process [8]. The ion concentration profiles for $Na^+$ and $K^+$ are close to the index profile only in glasses without heavy oxides like $PbO_2$, $ZnO_2$, $BaO_2$, *etc.* Strong diffusion of alkaline ions is

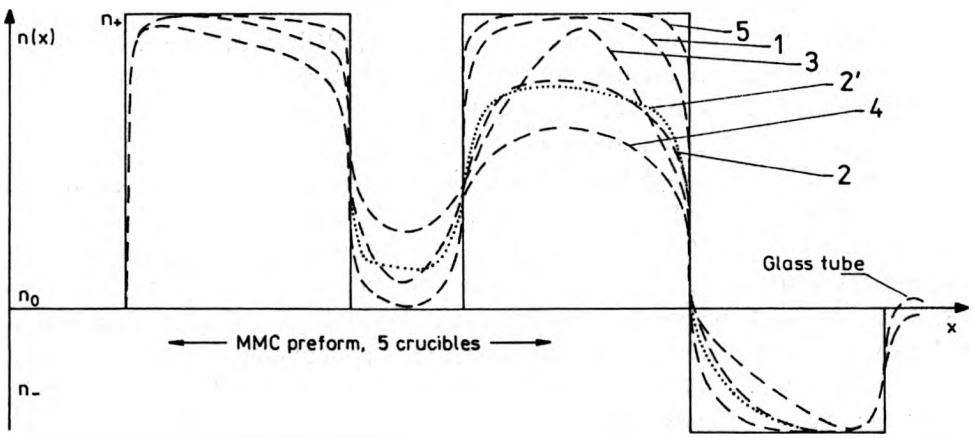


Fig. 3. Family of normalized, theoretical and measured, refractive index profiles of double-ring-index optical MMC preforms for fibers. Technological data concerning the processes leading to profiles 1–5 are presented in Tabs. 1 and 2. The discrepancy between curves 2–2' shows the accuracy of theoretical predictions of diffusion in multicrucible system against the measurement.

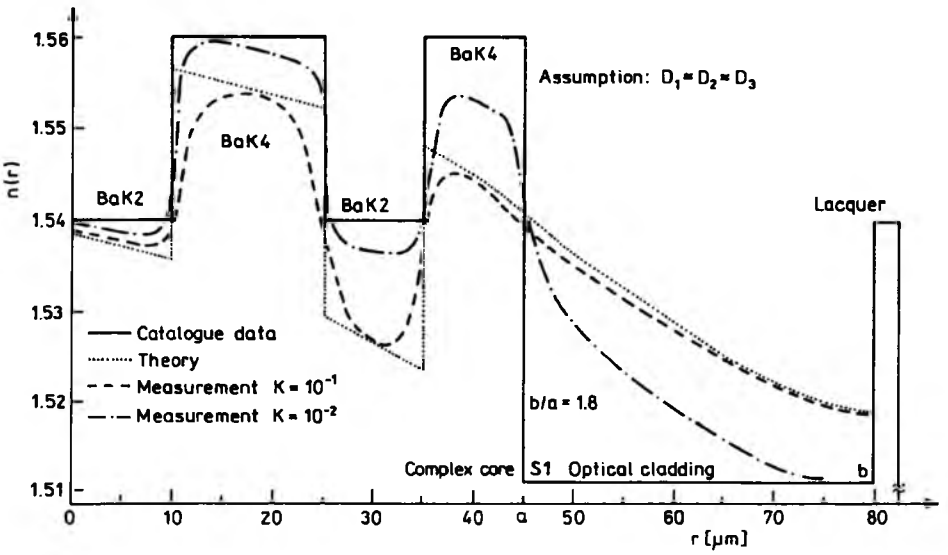


Fig. 4. Family of normalized, theoretical and measured, refractive index profiles of double-ring-index optical fibers. Another system of migrating ions, in comparison with Fig. 3. Glass system: BaK2-BaK4-BaK2-BaK4-S1 – polyimide lacquer ($n_i$ = 1.5392, 1.5612, 1.5130, 1.54). The internal dimensional proportions of this fiber are presented in Fig. 8. The outer cladding of this fiber is a source of $Na^+$ ions and the core regions are the source of $Ba^{2+}$. The measurements performed during a single process. The complex diffusion coefficients $K_i = D_i t/a_i^2 = \pi D_i l_d/Q_i$ were changed through the changes of process temperature $T$ and diffusion time $t_d$.

observed in nearly all ion systems. The influence of ion diffusion on the index profile is of the order $\Delta n \approx 0.01$–$0.03$. The observed diffusion profiles of $Na^+$ and $K^+$ were quite complicated and always influenced by mixed alkali effect.

The diffusion of heavy ions $Pb^{2+}$ and $Ba^{2+}$ during the MMC process has a profound impact on the fiber refractive index profile. These ions have, however, much lower values of constant $D$. In certain technological conditions, the difference of diffusion parameters between light and heavy ions can be diminished, which was observed in certain index profiles measured. In a compound glass, the index profile is determined by molar content of several $Me^{2+}$ ions. An increase in the temperature of MMC process did not cause the diffusion depth to increase, which was observed in flat geometry with the same glasses, and much longer diffusion time. Some core-cladding boundary effects were observed, where the concentration of main migrating ions increased anomalously, in certain technological conditions. The depth of migration was observed to decrease with process temperature near optimal fiber pulling conditions, which was caused by the change of glass viscosity, an increase in the velocity of glass passage through the inter-nozzle region and thus shorter diffusion time. The Reynolds number changes with temperature, and its value defines the stability of the pulling process. The value of this number and the optimal process temperature are chosen experimentally for each core-cladding glass system.

Table 1. Data for exemplary technological process of MMC preforms for hybrid MMC-RIT optical fibers

| Kind of optical fiber | Number of experiment (the same process) | Diameter of nozzle of axial crucible $\Phi$, [mm] | Approximate value of the ratio of nozzle diameters $\Phi_1:\Phi_2:\Phi_3:\Phi_4:\Phi_5:\Phi_6$ | Distance between nozzles $h_{12}, h_{23}, h_{34}, h_{45}, h_{56}$, [mm] | Heating lenght $L_h$, [mm] | Complex coefficient of diffusion $K=Dk/a^2$ [$m^2/s$] | Pulling speed $v$ [m/s] | Relative height of glass melt $H_1, H_2, H_3, H_4, H_5, H_6$ (stationary solution) | Number and location of termal zones; max. zonal temp. difference | Temperatures in furnace zone $T_1/T_2/T_3/T_4$ [°C] |
|---|---|---|---|---|---|---|---|---|---|---|
| Four crucibles, presented in Fig. 5b | 1<br>2<br>3 – exper.<br>3' – theor.<br>4<br>5 | 5 | 5:6.7:8.3:10 | 6 20 6 – –<br>6 20 6 – –<br>6 20 20 – –<br>6 20 20 – –<br>6 20 20 – –<br>6 20 6 – – | 10<br>10<br>10<br>10<br>50<br>10 | | 0.5–10 | strictly quasi-<br>quasi-<br>quasi-<br>quasi-<br>non-, $H_1$ low, $H_4$ high | two zones, $\Delta T_{max} = 40$ K, hot zone located on 4th crucible | 950/960<br>950/990<br>1050/1060<br>1050/1060<br>1100/1140<br>1000/1020 |
| Five crucibles, presented in Fig. 3 | 1<br>2 – exper.<br>2' – theor.<br>3<br>4<br>5 | 1.2 | 1:3:4:6:8 | 10 10 10 10 –<br>10 10 10 30 –<br>10 10 10 30 –<br>10 10 10 30 –<br>10 10 10 30 –<br>10 10 10 10 – | 10<br>50<br>50<br>50<br>50<br>10 | $10^{-2}$<br>$10^{-1}$ | 0.5–10 | strictly quasi-<br>quasi-<br>quasi-<br>quasi-<br>non-, supported high value of $H_4$ | three zones $\Delta T_{max} = 50$ K, middle narrow cool zone located on 4th crucible | 950/960/950<br>1100/1090/1100<br>1100/1090/1100<br>1100/1050/1100<br>1100/1050/1100<br>970/1000/950 |
| Six crucibles, presented in Fig. 6 | 1<br>2 | 5 | 5:5.5:6.7:<br>7.5:8.7:9.2 | 5 15 10 5 5<br><br><br>5 5 5 5 5 | 30<br><br><br>30 | | 0.5–10 | non-stationary, supported high value of $H_5$<br>quasi-stationary | four zones, the hottest zone on 2th–4th crucibles, the coolest zone on 5th crucible | 950/1010/930/970<br><br><br>950/960/970/980 |

T a b l e 2. The main stages of hybrid technological process for the manufacturing of MMC mono-mode optical fiber of complex refractive index profiles for transmission, functional and sensory applications. Exemplary technological data. In-process dimensions of preform and fiber sub-structures

| Number of stage d | | 1 | 2 | 3 | 4 |
|---|---|---|---|---|---|
| Name of process stage d | | MZD preform | RIT pre-process | RIT collapsing | Optical fiber |
| Process actions d | | MZD rod with designed RIP | MZD rod inserted in outer glass tube | Collapsed composite preform of optical fiber | Mono-mode optical fiber |
| Fiber sample name o | Type of RIP o | Approximate dimensions of structures during process $\Phi_i$, $h$, $r_i$, $\varphi$ [μm], [mm] | | | |
| Quadruple crucible Fig. 5b | Double *W* | 150/200/250/300 [μm] | $\Phi_{int} = 0.5$, $\Phi_{ext} = 3.5$, $h = 3$ [mm] | 0.3/3.1 [mm] | $r_1/r_2/r_3/r_4/r_5/r_6/\varphi$ [μm] 3/4/5/6/62.5 |
| Quintuple crucible Fiber from Fig. 3 | Double ring | 50/150/200/300/400 | $\Phi_{int} = 0.5$, $\Phi_{ext} = 3.5$, $h = 3$ [mm] | 0.4/3.1 | 1/3/4/6/8/62.5 |
| Six-fold crucible Fiber from Fig. 6 | Complex double *W* | 150/165/200/225/260/275 | $\Phi_{int} = 0.5$, $\Phi_{ext} = 3.5$, $h = 3$ [mm] | 0.3/3.1 | 3/3.3/4/4.5/5.2/5.5/62.5 |

($r_i$ – particular region radius, $h$ – glass tube wall thickness, $\Phi_i$ – particular region diameter, $\varphi$ – outside diameter of non-clad optical fiber, RIP – refractive index profile, MZD – multicrucible zone diaphragm, RIT – rod-in-tube process).

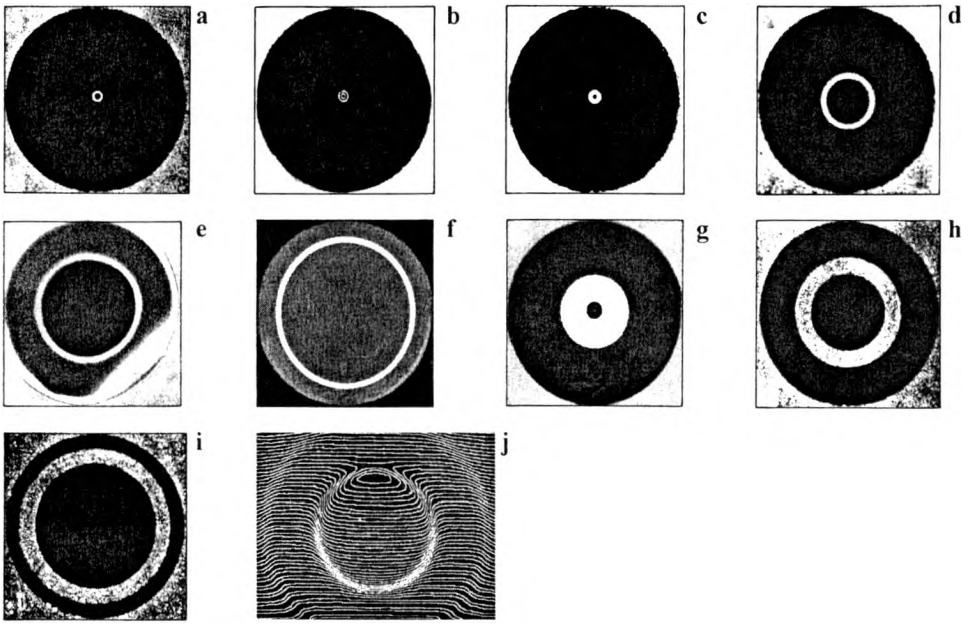


Fig. 5. Examples of MMC optical fibers of ring-index and double-ring-index profiles manufactured at Biaglass Fiber Optics Laboratory. Photographs of the fiber cross-sections. Data: $\Delta = 0.25\%$, $\Phi = 125$ μm for all single-mode fibers; $\Delta \approx 1\%$ for multi-mode fibers, relative ring-core thickness parameter $\eta = b_i/a_i$ (where $b_i$ and $a_i$ are bigger and smaller ring radii), $h = (b_i - a_i)/2$ – core ring thickness. **a** – $2b = 7$ μm, $2a = 4$ μm, $h = 1.5$ μm, $\eta = 1.75$, **b** – $2b_1 = 8$ μm, $2a_1 = 6$ μm, $2b_2 = 4$ μm, $2a_2 = 2$ μm, $\eta_{11} = b_1/a_1 = 1.3$, $\eta_{12} = 4$, $\eta_{22} = 2$, **c** – $2b = 9$ μm, $2a = 3$ μm, $\eta = 3$, **d** – $2b = 36$ μm, $2a = 30$ μm, $\eta = 1.2$, **e** – $2b = 75$ μm, $2a = 65$ μm, $\eta = 1.2$, **f** – $2b = 100$ μm, $2a = 92$ μm, $\eta \approx 1.1$, **g** – $2b = 50$ μm, $2a = 10$ μm, $\eta = 5$, $\Delta = 0.5\%$–$1.5\%$, multi-mode, **h** – $2b = 70$ μm, $2a = 50$ μm, $\eta = 1.4$, **i** – $2b = 105$ μm, $2a = 85$ μm, $\eta = 1.24$, **j** – Micro-interferometric imaging of ring-core region in an optical fiber; ring thickness $h = 3$ μm, $2b = 13$ μm, $2a = 7$ μm, $\eta \approx 1.86$.

The full manufacturing process of complex refractive index optical fiber consists of several stages and has hybrid nature. These stages are indicated, for an exemplary fiber, in Tab. 1, with technological data given in Tab. 2. The index profiles of the fibers from the tables are presented in Figs. 3 and 4. The MMC preform rods, of ready refractive and geometrical structure, are inserted into a glass tube of fit, inside and outside, dimensions. This set gives, after thinning, ready fiber of complex structure and standardized dimensions. The latter stage is called rod-in-tube (referred to as RIT). Standardized outside dimensions are necessary to facilitate fiber measurements. The fiber internal structure may be further complicated by the use of multi-rod-in-tube method, leading to, for example, ring-index, highly birefringent (HB) optical fibers. With the hybrid MMC-RIT method, several samples of single-mode and multi-mode ring-index optical fibers of different geometrical and refractive parameters were pulled. The practice shows that the hybrid method allows us to combine glasses of comparatively distant thermal and mechanical characteristics, which broadens the choice of glasses for desired ion system.

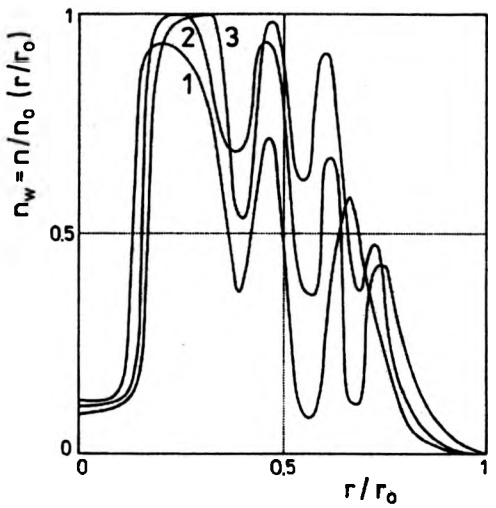


Fig. 6. Measured refractive index profiles of a single-mode triple-ring-index optical fiber analogous to that of double-ring-index from Fig. 5b for different stages of the MMC batch pulling process. 1 – beginning, 2 – middle, 3 – end. Imaging through the whole cross-section from fiber axis. $2r_0 = 2a = \varphi_{core}$ – ring-core diamater.

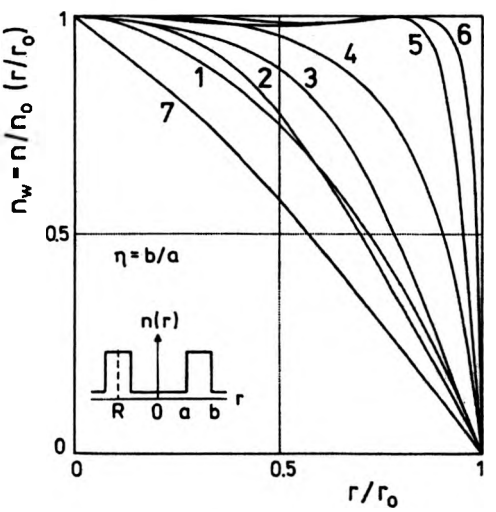


Fig. 7. Measured and calculated refractive index profiles of multi-mode ring-index fiber $n(r) = n_1(1-2\Delta(|r-r_0|/|b-r_0|)^{\alpha})^{1/2}$ for $2r_0 - b \le r \le b$, $n(r) = n_1(1-2\Delta)^{1/2}$ outside ring-core, of optimal $\alpha$ profile parameter obtained with the WKB method $\alpha \approx 1-(n_1/N_1)(\lambda/\Delta)(d\Delta/d\lambda)$, $N_1 = dk_1/dk$. Curve 1 – parabolic $\alpha = 2$, curve 2 – $\alpha = 5$, curves 3 and 4 – measured gradient profiles, curves 5 and 6 – measured quasi-step-index profiles, curve 7 – triangular profile $\alpha \approx 1$, $R = r_0 = 0.5(a+b)$. Imaging only for ring-core region of the fiber. Quite similar gradient index profiles inside the ring-core can be built into single-mode MMC fibers. Here, $R$ is the radius of core ring center and $r_0 = b-a$, thus the refractive characteristics are presented only for half core rings, because of being symmetrical aganist the value of $R$.

Figure 5 presents photographs of the kinds of manufactured fibers, analysed theoretically and measured in this work. In particular, investigations focused on subtle details of index profiles. Some fibers had considerable values of parameter $\Delta$, where $\Delta = (n_1^2 - n_2^2)/n_2^2 \approx 1 - n_2/n_1$, exceeding 1% and extremely narrow, local refractive dips, of the order from several micrometers to below a single micrometer. The ability to build very narrow and stable refractive layers into a fiber has a basic meaning to the tailoring of fiber dispersion and effective area. Measured families of ring-index fiber profiles are depicted in Figs. 3, 4, 6 and 7. The dimensional stability, analysed both theoretically and experimentally, of the batch MMC process is shown in Fig. 8.

Some of the general conclusions of research on fiber profiling are: a batch technique requires control of liquid glass level in the crucibles in order to prevent changes in fiber geometry, terminal part of the batch process is influenced by the shape of crucible bottom (which can be flat, parabolic, cylindrical, or conical), it is possible to combine core-cladding system of glasses of as distant thermal and mechanical characteristics as 15% and more, the profile is determined by migration of dominating ions, and inter-nozzle distances at optimal process temperature, distinctive diffusion of $Pb^{2+}$ and $Ba^{2+}$ ions is observed in the fiber, pre-setting of initial glass levels for stationary outflow stabilizes the batch technology on condition that the relative active

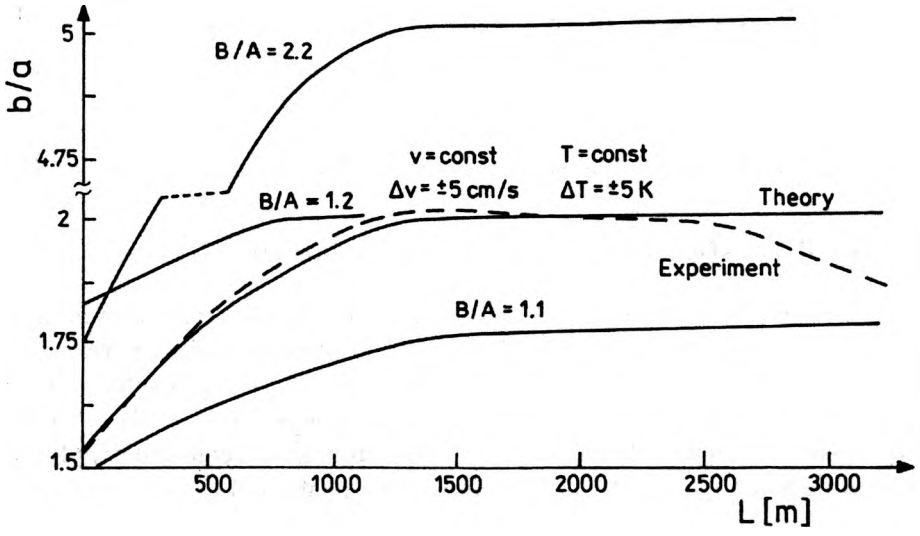


Fig. 8. Changes in the relative dimensions of multi-layered MMC optical fibers calculated theoretically (solid lines) and measured during fiber pulling (broken line) for different stages of a single batch process. Different curves are for a few sets of relative crucible nozzle dimensions and heights of molten glass in crucibles. The parameters of the process were: $T$ = const, $\Phi$ = const, the values of $\eta_i$ and $\rho_i$, were chosen experimentally, $h_1/h_2 = 2$, furnace temperatures kept within the following region $\Delta T \approx \pm 5$ K, fibre pulling speed kept within the following region $\Delta v \approx \pm 5$ cm/s, $B/A$ – theoretically calculated asymptotes for fiber dimensions for constant dimensional proportions between successive nozzles [8], $b/a$ – cladding/core proportions, $L$ [m] – fiber length, since the pulling speed is constant, the abscissa shows also the fiber pulling time $t$ [s].

surfaces of molten glass system stay invariant, effect of mixed alkalis may be used during the fiber pulling process to equalize the involved ion mobilities of distant dimensions, it is possible to obtain profile details of dimensions comparable to the optical wavelength.

## 3. Chosen properties of ring-index optical fibers

The ring-index optical fibers are characterized by minimal value of refraction at the optical filament axis. Fiber parameters are: magnitude of central refractive depression in geometrical and refractive sense, relative thickness of refractive ring core against the value of $\lambda$. The refractive profile of step ring-index fiber is $n(r) = n_1$ for $a \le r \le b$ and $n(r) = n_2$ outside this region (central depression and outer cladding). Let us introduce a parameter $\eta = b/a$ which is a normalized thickness of ring core. Let us assume that $\Delta \approx 1 - n_2/n_1 \ll 1$ and the fiber propagates TEM wave. In such a case the electrical field can be presented in the following form for the consecutive regions of fiber (central depression, core and outer cladding):

$$E_m^y = C_1 I_m(W)\cos(m\theta), \quad \text{or}$$

$$E_m^y = C_1 I_m(W)\sin(m\theta), \quad W = \frac{wr}{\eta a} = \left(\frac{w}{\eta}\right)\left(\frac{r}{a}\right) \quad \text{for } 0 \le r \le a, \tag{4}$$

$$E_m^y = [C_2 J_m(U) + C_3 N_m(U)]\cos(m\theta), \quad \text{or}$$

$$E_m^y = [C_2 J_m(U) + C_3 N_m(U)]\sin(m\theta), \quad U = \frac{ur}{\eta a} \quad \text{for} \quad a \le r \le b, \tag{5}$$

$$E_m^y = C_4 K_m(W\eta)\cos(m\theta), \quad \text{or} \quad E_m^y = C_4 K_m(W\eta)\sin(m\theta) \quad \text{for} \quad b \le r. \tag{6}$$

where $C_i$ are amplitude constants, $I_m$, $J_m$, $N_m$, $K_m$ are Bessel functions of first and second kind $m$-th order, $u$, $w$ are Bessel function arguments and $V$ normalized frequency expressed with classical equations, here adapted to the geometry of ring -index fiber $u^2 = b^2k^2(n_1^2 - \beta^2k^{-2})$, $w^2 = b^2k^2(\beta^2k^{-2} - n_2^2)$, $V^2 = b^2k^2(n_1^2 - n_2^2)$, $k = 2\pi/\lambda$, $m$ – azimuthal modal number, $\eta = b/a$, $\beta$ – propagation constant. Applying boundary conditions to Eqs. (4)–(6) one gets the eigen-equation of ring-index optical fiber

$$\frac{wK_{m+1}(w)}{uK_m(w)} = \frac{A+B}{C+D} \tag{7}$$

where:

$$A = uI_m\left(\frac{w}{\eta}\right)\left[J_{m+1}(u)N_{m+1}\left(\frac{u}{\eta}\right) - J_{m+1}\left(\frac{u}{\eta}\right)N_{m+1}(u)\right],$$

$$B = wI_{m+1}\left(\frac{w}{\eta}\right)\left[J_{m+1}(u)N_m\left(\frac{u}{\eta}\right) - J_m\left(\frac{u}{\eta}\right)N_{m+1}(u)\right],$$

$$C = uI_m\left(\frac{w}{\eta}\right)\left[J_{m+1}\left(\frac{u}{\eta}\right)N_m(u) - J_m(u)N_{m+1}\left(\frac{u}{\eta}\right)\right],$$

$$D = wI_{m+1}\left(\frac{w}{\eta}\right)\left[J_m\left(\frac{u}{\eta}\right)N_m(u) - J_m(u)N_m\left(\frac{u}{\eta}\right)\right].$$

For obvious reasons, this equation, for $\eta \to \infty$, undergoes transformation to a classical eigenequation of weakly guiding cylindrical optical fiber. A few families of numerically calculated solutions to this equation, for different values of parameter $\eta$, are presented in Fig. 9**a**–**d**. These calculations were performed for fibers of geometries shown in Fig. 5**a**–**c**.

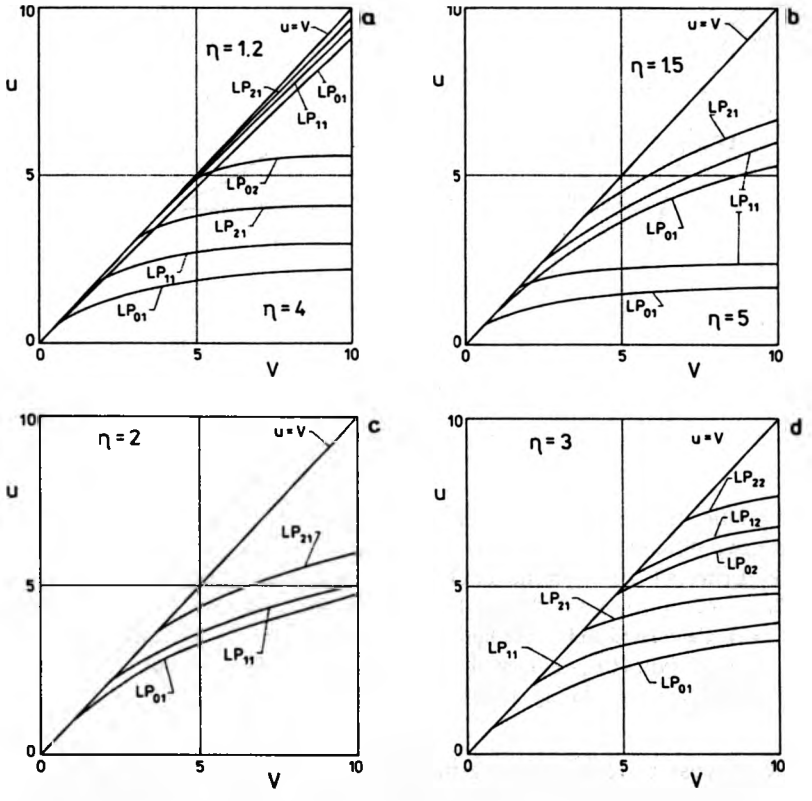


Fig. 9. Calculated modal characteristics $u(V)$ and cut-off conditions $u(\mathrm{LP}_{lm}) = V$ for several different values of ring-core parameter $\eta$ and several lowest order LP modes; $u$ – wave argument, $V$ – normalized frequency. **a** – $\eta = 1.2$ and $\eta = 4$; upper family of curves correspond to the value of $\eta = 1.2$ while the lower one to $\eta = 4$, **b** – $\eta = 1.5$ and $\eta = 5$; upper family of curves correspond to the value of $\eta = 1.5$ while the lower one to $\eta = 5$, **c** – $\eta = 2$, **d** – $\eta = 3$.

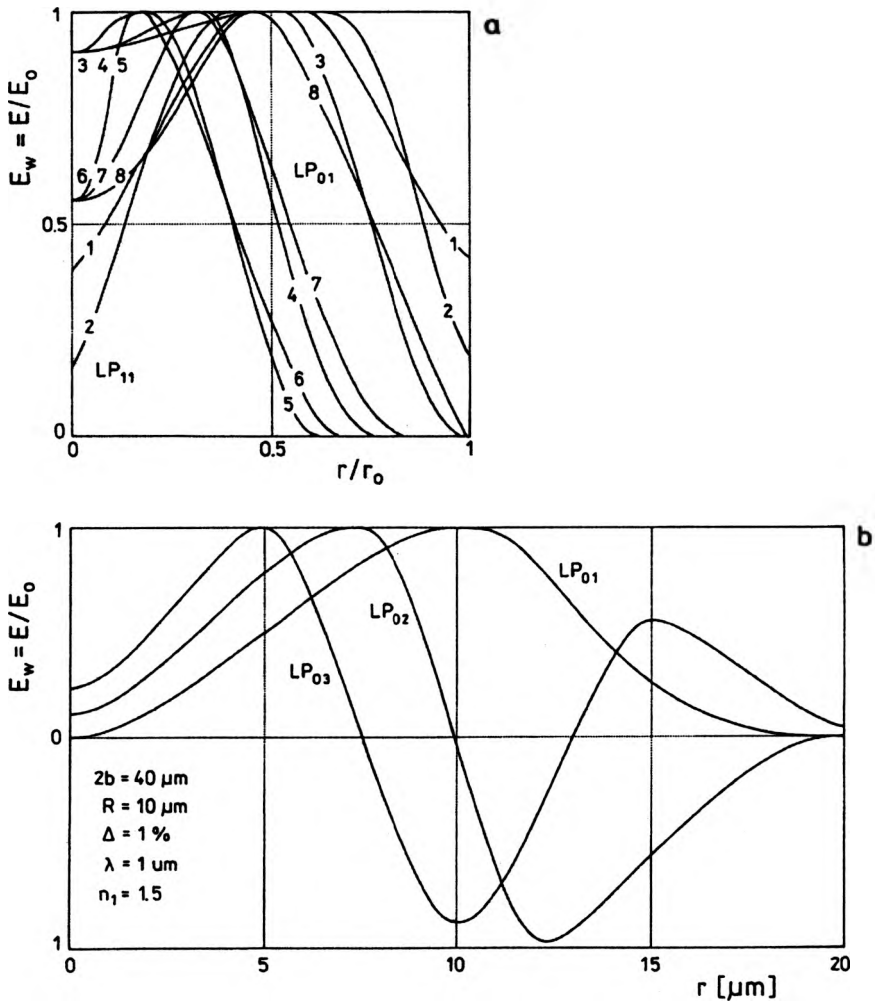


Fig. 10. Calculated field profiles for the fundamental $LP_{01}$ and next order $LP_{11}$ mode as functions of ring-core parameter $\eta$ for two different values of normalized frequency under the cut-off condition $V_1 = V_c(LP_{11})$, $V_2 = V_c(LP_{21})$, curves 1 and 2 – profiles of $LP_{11}$ mode for $V_1$ and $V_2$, curves 3, 4, 5 – profiles of $LP_{01}$ mode for $\eta = 1.2$, $\eta = 1.5$, $\eta = 3$, $\Delta = 0.5\%$, $\lambda = 1$ μm, $n_2 = 1.5$, $V_1$, curves 6, 7, 8 – similarly to curves 3, 4, 5 but for $V_2$ (**a**). Calculated field distributions of higher order, cylindrically symmetric, minimum field value on the fiber axis, ($LP_{m1}$ modes of $m = 0$, $l = 1, 2, 3$) in an exemplary, low order mode, ring-index optical fiber. Supplement to Fig. 10**a** (**b**).

The mode of the lowest order in a ring-index optical fiber is $LP_{01}$ which is equivalent to $HE_{11}$. The next mode is $LP_{11}$, equivalent to either $TE_{01}$, $TM_{01}$ or $HE_{21}$. With an increase in the parameter $\eta$, for chosen value of normalized frequency $V$, from the asymptotic value of 1 to the infinity the ring-index optical fiber resembles modally, more and more, a classical optical fiber. While decreasing the $\eta$ to unity, for $V$ = const, the number of propagated modes in ring-index fiber decreases. Figure 10**a** shows

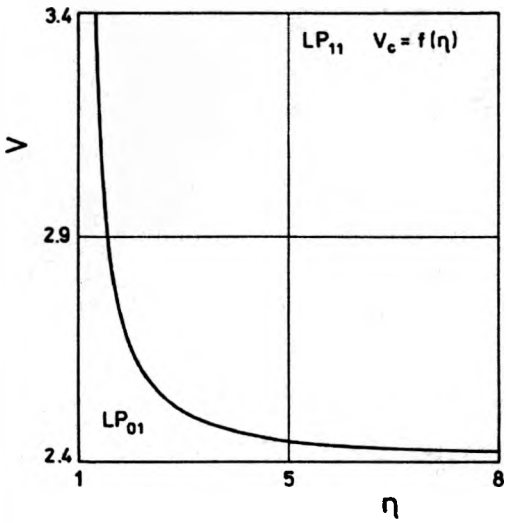


Fig. 11. Calculated single-mode condition of ring-index optical fiber as a function of normalized ring-core parameter η

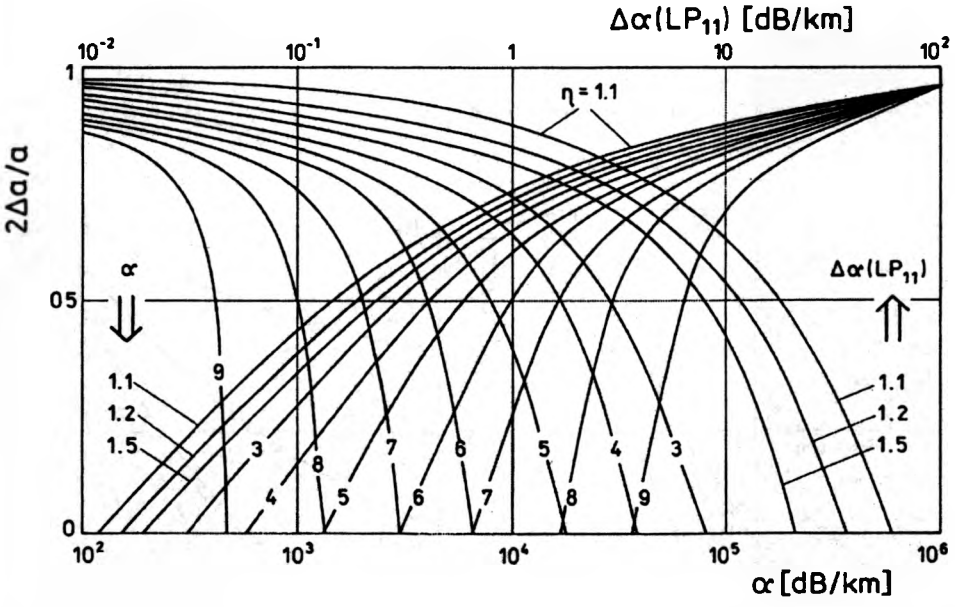


Fig. 12. Calculated characteristics of lossy discrimination of $LP_{01}$ mode in order to obtain a condition of quasi-single-mode propagation of $LP_{11}$ mode (first set of curves α [dB/km], with lower axis of abscissa). A lossy central refractive depression is introduced with α [dB/km] and relative thickness $\Delta a/a$. As a result, the introduced intentional losses of $LP_{01}$ mode are of the order of 50 dB/km. The accompanied, not intentional, excess losses for the $LP_{11}$ mode are Δα [dB/km] (second set of curves, with upper axis of abscissa), $a$ – radius of axial refractive depression, $\Delta a$ – radius of axial lossy region, α – necessary refractive depression material losses to obtain 50 dB/km discrimination of the $LP_{01}$ mode.

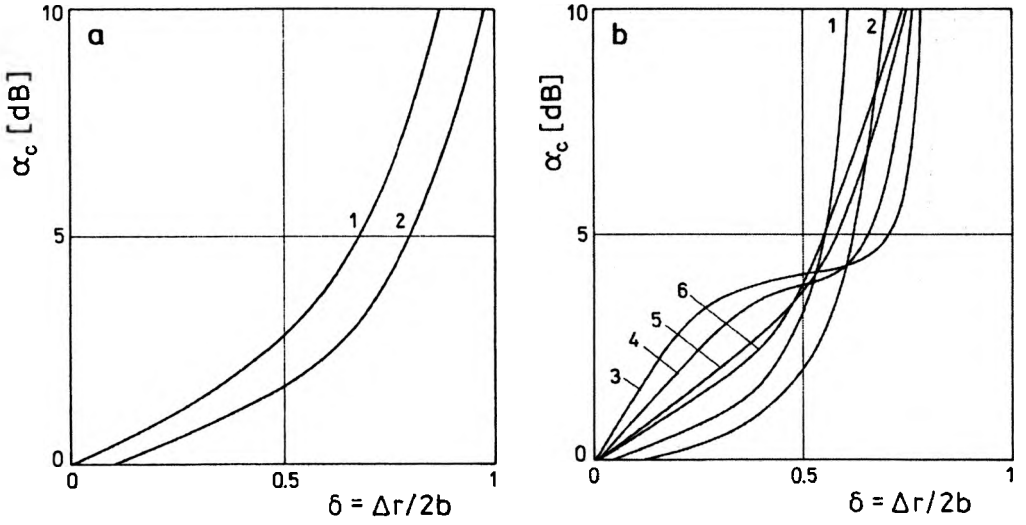


Fig. 13. Measured coupling losses $\alpha_c$ [dB] versus relative lateral displacement $\delta = \Delta r/2b$, ($\Delta r$ – real displacement along $r$ axis) for classical and ring-index optical fibers as a measure of field diameter. **a** – single-mode, **b** – multi-mode. Parameters: **a** – curve 1 – step-index classical single-mode optical fiber for optical communications in the first window, $2a = 9$ μm, $V = 2.5$, $\lambda = 1.3$ μm; curve 2 – ring-index single-mode optical fiber: $2b \approx 9$ μm, $2a = 3.5$ μm, $V = 2.5$, $\lambda = 1.3$ μm, **b** – curve 1 – classical, multi -mode, step-index fiber, $2a = 50$ μm, NA = 0.18, curve 2 – classical, multi-mode, step-index fiber, NA = 0.25, curves 3–6 – multi-mode step-ring-index fibers, curve 3 – $\eta = 2$, $2b = 50$ μm, curve 4 – $2b = 50$ μm, $\eta = 3$, curve 5 – $\eta = 5$, curve 6 – $\eta = 10$.

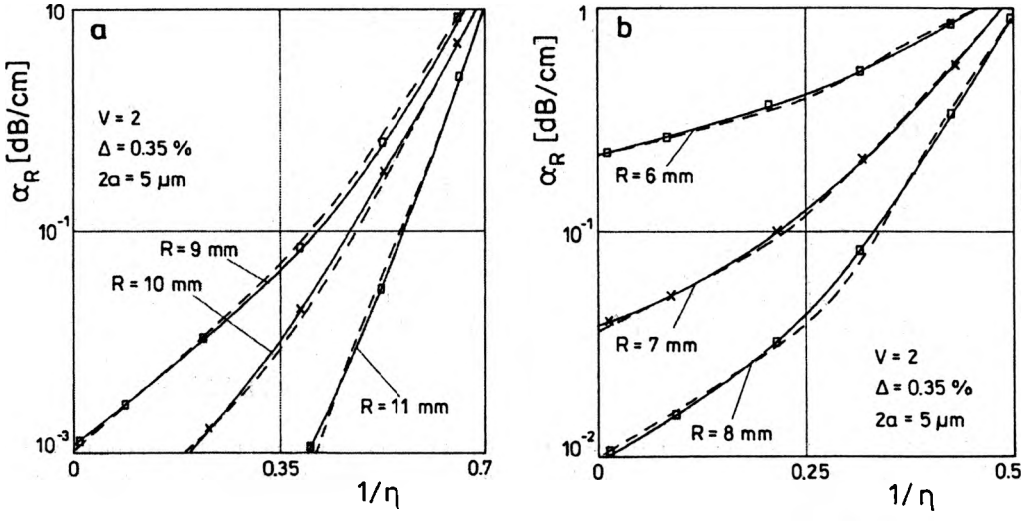


Fig. 14 **a**, **b**. Calculated (broken curves) and measured (solid curves) incremental loss $\alpha_R$ characteristics of ring-index optical fibers as functions of normalized core parameter $1/\eta = a/b$ for several values of fiber bending. $\Delta = 0.35\%$, $2a = 5$ μm, $V = 2$, bending radiuses $R = 11$–6 mm.

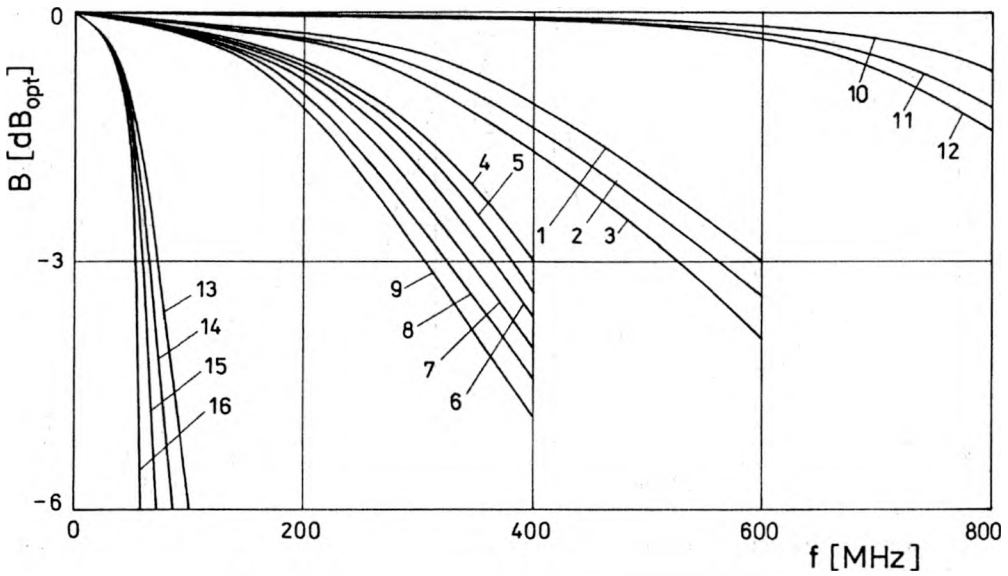


Fig. 15. Measured bandwidth $B$ for several groups of single-mode and multi-mode, low-loss ring-index optical fibers manufactured during the MMC process at GW Biaglass. Technical data: $L \approx 1$ km, $\lambda \approx 1$ μm, $S = 14$ dB/km, curves 1–3: $\alpha \approx 1.8$–$2.3$, $2b = 50$ μm, $R = 13$–$16$ μm, curves 4–9: $\alpha \approx 1.1$–$1.3$, $2b \approx 62.5$ μm, $R = 13$–$16$ μm, curves 10–12: single-mode optical fibers, $\alpha \approx 4$–$6$, $2b = 7$ μm, $2a = 4$ μm, $\Delta = 0.25$–$1.75\%$, curves 13–16: step-ring-index multi-mode fibers $2b = 50$–$60$ μm, $2a = 10$ μm, $\eta = 5$–$6$, $\Delta = 0.5$–$1.5\%$.

calculated modal field distributions for $LP_{01}$ and $LP_{11}$ in the cross section of a ring-index optical fiber in the case of $LP_{11}$ cut-off (curves 3, 4, 5) and $LP_{21}$ cut-off (curves 6, 7, 8). Figure 10**b** shows calculated field distributions for higher order modes in ring-index optical fiber. The value of $\eta$ alone does not exhaust the description of single-mode ring-index fiber but yet strongly influences the modal characteristics.

Ring-index optical fibers can be divided into two major classes, of central refractive depression comparable to the wavelength $2a \approx \lambda$ and much larger than the wavelength $2a \gg \lambda$. The second group, especially for large values of $2a$ is expected to propagate quasi-planar modes, as in bent optical planar waveguide. The circumference of the core carries standing planar wave and the propagation goes on along the fiber. The first group of ring-index fibers can work in two fundamental wave conditions: 1 – through the choice of such parameters as $V$ and $\eta$ for single-mode propagation of $LP_{01}$ (which is presented in Fig. 11), 2 – through the introduction of sufficiently high optical losses of the central refractive depression and, thus, lossy discrimination of $LP_{01}$ mode (which is presented in Fig. 12). The differential loss stems from considerably distant shapes of evanescent modal fields between $LP_{01}$ and $LP_{11}$ in the depression region. In the first case, the ring-index fiber of the first group is single-mode for $LP_{01}$, and in the second case it is quasi-single-mode for $LP_{11}$. In the latter case, the fiber works at larger values of normalized frequencies than at single-mode conditions.

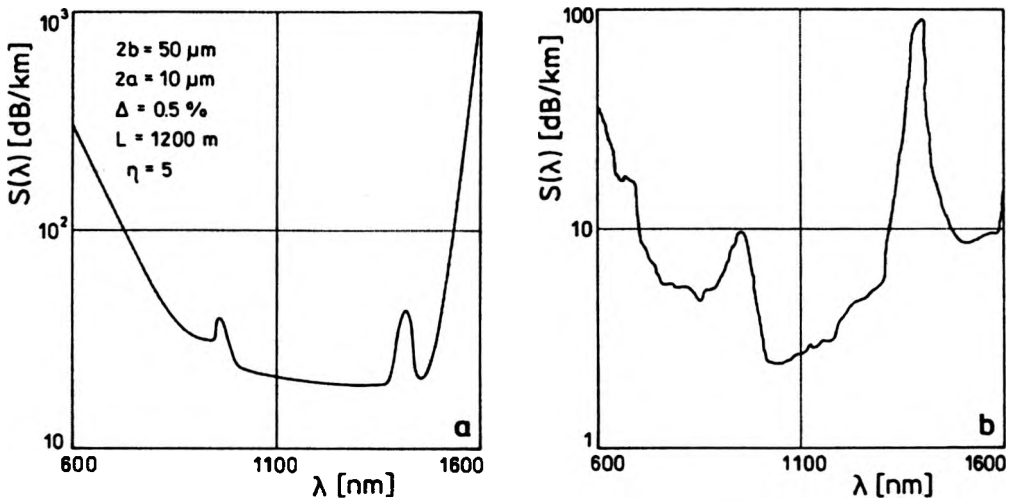


Fig. 16. Measured spectral attenuation $S(\lambda)$ characteristic of an exemplary multi-mode MMC gradient-ring-index optical fiber. Fiber from photograph in Fig. 5**g**, $\alpha \approx 3.9$ (**a**). Measured spectral attenuation $S(\lambda)$ characteristic of an exemplary single-mode MMC ultra-low-loss step-index optical fiber, $2b = 8$ μm, NA = 0.12 (**b**).

The cut-off value of normalized frequency for $LP_{11}$ mode, *i.e.*, $V_c(LP_{11})$ is obtained from the eigenvalue equation (7), assuming $u = V$ (or $n_{eff}(LP_{11}) = n_2$) for modal arguments or effective indices, treating $\eta$ as a solution parameter. Figure 11 shows the calculated region $V_c(LP_{11}) = f(\eta)$ of single-mode solutions, where $V_c$ is the cut-off value of the normalized fequency. The ring-index optical fiber is single-mode for $LP_{01}$ in the region $V(\eta)$ under the depicted curve. When the core ring parameter $\eta$ decreases asymptotically to unity, the value of normalized frequency may be chosen much larger than 2.405 – cut-off for $LP_{01}$ in classical fiber. Figure 10**a** presents calculated modal profiles in the ring-index fiber. The comparison with modal profiles (actually modal field diameters) of analogous classical fiber (the same values of $\Delta$ and $V$) reveals that the field in ring-index fiber extends deeper outside the core into central depression and outer optical cladding. The field extends even deeper for $\eta \to 1$ revealing bigger and bigger difference compared to classical fiber. As a result, a single-mode ring-index optical fiber has theoretically lower coupling losses (curve 2) with active photonic components and among themselves, as compared to classical single-mode fiber (curve 1), which has been measured and presented in Fig. 13**a**, but it is more susceptible to micro-bending than classical fiber (Fig. 14**a**, **b**). The coupling characteristics of multi-mode ring-index optical fibers, measured and presented in Fig. 13**b**, have strong flexion point for the offset around the core radius. These characteristics (curves 3–6) are compared with coupling ones for classical fibers (curves 1 and 2).

Several samples of practically performed single-mode and multi-mode MMC ring-index optical fibers have been measured for bandwidth $B$ and attenuation $S$, and the results are shown in Figs. 15 and 16. In the case of step-index and gradient-index

multi-mode fibers, photographed in Fig. 5**g**, the difference with classical one is nearly to be omitted. The measured dispersion of multi-mode gradient ring-index optical fiber, for $\eta \approx 1.5$, $\lambda = 0.85$ μm, $\Delta = 0.5\%$, analogous to the one in Fig. 5**g** was around 500 MHz×Km. The measured dispersion of single-mode ring-index optical fibers was in the range 1.5–5 GHz×Km, depending on the fiber geometry and index profile. Figure 16**a**, **b** show typical spectral losses of multi-mode and single-mode low-loss MMC optical fibers, respectively. These values can be obtained with this technology for off-shelf products, and high silica ultra-pure SLS or SBS glasses.

## 4. Conclusions

This work recalls, reveals and summarizes some of the characteristic features of ring-index optical fibers. It was shown that the MMC process allows effective manufacturing of ring-index fibers from two basic single-mode families, with small and large core rings (Fig. 5). Single, double and triple ring-index sample fibers have been manufactured (Figs. 3, 4, 6 and 7). Modal eigen-characteristics show that the normalized ring-core parameter $\eta$ has an essential impact on the signal behaviour of the fiber (Fig. 9). The ring profile favours propagation of the $LP_{11}$ mode and other modes of ring symmetry and minimal field value on the fiber axis (Fig 10). Unlike the classical fiber, the ring-index one can be single-mode even for large values of normalized frequencies exceeding the boundary of $V = 2.405$. With ring-core parameter $\eta$ approaching asymptotically the unity, the $V$ value can be practically as large as 3–6, while the fibre still maintains single-mode condition (Fig. 11). Quasi-single-mode propagation condition is obtained in a ring-index fiber through the lossy discrimination of the fundamental mode (Fig. 12). Single-mode ring-index fibers have larger effective field diameters. For the same fiber parameters, this has been shown through direct measurements in Fig. 13**a**. Multi-mode ring-index fibers have bigger coupling losses for small lateral offsets and smaller coupling losses for large lateral offsets than classical multi-mode optical fibers of analogous parameters (Fig. 13**b**). The bending losses of ring-index single-mode fibers are bigger than in classical ones (Fig. 14). The bandwidth of multi-mode optical fibers is only slightly influenced by the refractive ring. In single-mode fibers the refractive dip influences strongly the field diameter, causing the field to enter deeper into the cladding. The dispersion strongly depends on the details of the profile. The measurements on available single-mode samples showed the bandwidth to vary between 1.5–5 GHz×Km (Fig. 15). The prepared and measured samples of ring-index fibers had moderate spectral losses, in comparison with the CVD fibers, due to the characteristics of the MMC process. It seems that the ring-index fibers may find numerous applications in photonic communication and instrumentation systems in the nearest future.

*Acknowledgments* – The technology and measurements of ring-index optical fibers were all done in close cooperation with Prof. Jan Dorosz from Białystok University of Technology at Biaglass Fiber Optics Laboratories.

## References

[1] HECHT J., *Understanding Fiber Optics*, Prentice Hall, NJ, USA 1999.
[2] Web resources: www.dwdm.org, www.optics.org, www.osa.org, www.spie.org, www.fiberoptics.com, www.itu.org, www.ieee.org/leos.
[3] AGRAWAL G. P., *Nonlinear fiber optics*, [In] *Quantum Electronics Series*, Academic Press, CA, USA, 1995.
[4] NEUMANN E. G., *Single Mode Fibers, Fundamentals*, Springer-Verlag, Berlin, 1998.
[5] IZAWA T., SUDO S., *Optical Fibers: Materials and fabrication*, [In] KTK Scientific Publishers, Tokyo, 1997.
[6] DOROSZ J., *Multicore optical fibers manufacturing, Theoretical and practical aspects*, (in Polish), [In] Sci. Thes. Series, Technical University of Białystok, 1997.
[7] *Fiber Optics*, Application Notes and Product Catalogue, [Eds.] J. Dorosz, R. Romaniuk, Biaglass Co., Białystok, Warszawa, 1999 – 2000.
[8] ROMANIUK R., *Studies on tailored optical fibers*, (in Polish), [In] Sci. Thes. Series, Warsaw University of Technology, 2001, submitted for publication.

*Received October 9, 2000*